DERIVATION OF A SHARP-DIFFUSE INTERFACES MODEL FOR SEAWATER INTRUSION IN A FREE AQUIFER. NUMERICAL SIMULATIONS*

C. CHOQUET†, M. M. DIÉDHIOU†, AND C. ROSIER‡

Abstract. We derive a new model for seawater intrusion phenomena in free aquifers. It combines the efficiency of the sharp interface approach with the physical realism of the diffuse interface one. More precisely, a phase field is used as an intermediate variable for including the exchanges between the characteristic layers of the aquifer (salt water, fresh water, unsaturated zone). The three-dimensional problem is reduced to a two-dimensional model involving a strongly coupled system of PDEs of parabolic type describing the evolution of the depths of the two free surfaces. The model is discretized by finite elements in space and by a semi-implicit Euler method in time. Numerical simulations present some physical predictions from the model.

Key words. seawater intrusion, free boundaries, nonlinear parabolic PDE, system of strongly coupled PDEs, numerical simulations, finite elements

AMS subject classifications. 35R35, 35K20, 76S05, 76T05, 76E19, 65M60

DOI. 10.1137/15M102099X

1. Introduction. Groundwater is a major source of water supply. In coastal zones there exist hydraulic exchanges between fresh groundwater and seawater. They are slow in "natural conditions" and thus are often forgotten and replaced by a quasi-equilibrium between two fluid layers (Ghyben–Herzberg approximation). The picture fails in case of more drastic conditions due to meteorological events or to human interventions. Intensive extraction of freshwater leads for instance to local water table depression causing problems of saltwater intrusion in the aquifer. We thus need efficient and accurate models to simulate the displacement of saltwater fronts in coastal aquifers for the optimal exploitation of fresh groundwater.

We refer to the textbooks [6], [7], [8] for general information about seawater intrusion problems. Beyond the abovementioned Ghyben–Herzberg static model, the existing models for seawater intrusion may be classified into three categories.

Hidden diffuse interfaces: This is the physically correct approach. Fresh and salt water are two miscible fluids. Due to density contrast they tend to separate into two layers with a transition zone characterized by the variations of the salt concentration. Moreover the aquifer has to be considered as a partially saturated porous medium. There is another transition zone between the completely saturated part and the dry part of the reservoir, the definition of the area of desaturation being difficult. The whole problem is modeled by a convection-dispersion system for multicomponent mixtures in an unsaturated porous medium. Two "diffusive interfaces" are thus hidden in this kind of model. The approach is very cumbersome, both in theoretical and numerical terms ([13]; see also [4] when further assuming a saturated medium; see [1] for numerical recipes).

Hidden sharp interfaces: A first simplification consists in assuming that fresh and salt water are two immiscible fluids (see [13] in unsaturated media). Points where the salty phase disappears may be viewed as a sharp interface. Nevertheless the explicit tracking of the interfaces remains unworkable to implement without further assumptions (they correspond to the disappearing of an unknown and thus to the degeneration of the corresponding equation).

Sharp or abrupt interfaces: This approach is also based on the hypothesis that the two fluids are immiscible. Moreover the domains occupied by each fluid are assumed to be separated by a smooth interface called a sharp interface, no mass transfer occurs between the fresh and the salt area, and capillary pressure effects are neglected. This approximation is often reasonable (see, e.g., [6] and below).

Of course, this type of model does not describe the behavior of the real transition zone but gives information concerning the movement of the saltwater front. The other price to pay for this simplified approach is the mathematical handling of free interfaces.

In the present work we essentially have chosen to adopt the (numerical) simplicity of a sharp interface approach. We compensate for the mathematical difficulty of the analysis of the free interfaces by an upscaling procedure which allows us to model the three-dimensional problem (3D) by a PDE system set in a two-dimensional (2D) domain. The originality and novelty is to mix this abrupt interface approach with a phase-field approach, thus reinjecting in a new way the realism of diffuse interfaces models. We exploit here the specificity of the dynamics of the fluids in an aquifer for using such a model which was originally developed for phase transition phenomena in binary fluids. We thus combine the advantage of respecting the physics of the problem and that of the computational efficiency. The two key assumptions are summarized as follows:

- There is no explicit mass transfer between freshwater and saltwater, thus they are separated by an abrupt interface. The free interfaces are treated by an upscaling procedure, with an obvious dimensional gain since the 3D reality is processed by a 2D model. Both the simplicity and the efficiency of the model lie in the fact that the mass exchanges are in fact "hidden" in the diffuse interface.
- We suppose the existence of a diffuse interface between fresh and salt water. This diffuse interface is modeled using a phase-field approach, here an Allen–Cahn type model in fluid-fluid context.

The same process is applied to model the transition between the saturated and unsaturated zones.

In section 2, we detail the derivation of the model for the evolution of the depth h of the interface between freshwater and saltwater and of the depth H of the interface between the saturated and unsaturated zone. The approach is based on the conservation principles coupled with Darcy's law. Instead of closing the corresponding PDE system with the classical Fick's law assumption, we exploit the layered structure of the aquifer (Dupuit's setting) for upscaling the problem and we superimpose a 3D phase-field model for the mixing zone. The resulting model consists in a system of strongly and nonlinearly coupled PDEs of parabolic type. From the numerical viewpoint, the advantage of the sharp interface approach is of course the dimensional gain. Nevertheless the tracking of interfaces, even in an immiscible context, is a challenging problem (see, for instance, [31] and the references therein for the weaknesses of classical level-set or volume-of-fluid approaches). Here instead we benefit from the conservative structure of the model. We emphasize that we can demonstrate a logical

maximum principle from the point of view of physics (see [14]), which is not suitable in the case of sharp interface approximation (see, for instance, [18], [32]). Moreover the coupling of the Allen–Cahn model with the upscaled conservation equations avoids the classical weakness of the Allen–Cahn solutions: nonconserved fields. This seemingly nonnatural property does not appear in our final model. We thus do not need to consider more complex phase-field models, such as, for instance, a Cahn–Hilliard variant with degenerate mobility and logarithmic terms in the free energy. We either have to use a nonlocal Allen–Cahn equation with a time or a space-time dependent Lagrange multiplier to enforce conservation of mass (see [25]).

In section 3, we illustrate the numerical efficiency of the derived model. After a brief presentation of the discretization scheme, we compute various physical predictions from the model. In particular, for showing that our model retains the advantages while overcoming the weaknesses of the sharp interface approach and of the 3D exact model, we focus on two physical phenomena. We show that our upscaled model easily includes the potential compressibility of the fluids and of the rock, in contrast to the cumbersome 3D model [13], especially in the unsaturated setting which leads to fully degenerate equations. We also show that the coupling with the diffuse interface approach lets us properly treat cases where the mixing zone induces nonnegligible flow [15].

2. Derivation of the model. The basis of the modeling is the mass conservation law for each "species" (fresh and salt water) coupled with the classical Darcy law for porous media. Fluids and soil are considered to be weakly compressible.

For the 3D description, we denote by (x, z), $x = (x_1, x_2) \in \mathbb{R}^2$, $z \in \mathbb{R}$, the usual coordinates. The z-basis unit vector is e_z.

2.1. Conservation laws. We begin with the conservation of momentum. In view of the (large) dimensions of an aquifer (related to the characteristic size of the porous structure of the underground), we consider a continuous description of the porous medium. The effective velocity q of the flow is thus related to the pressure P through the so-called Darcy law

$$q = -\frac{k}{\mu}(\nabla P + \rho g e_z),$$

where ρ and μ are, respectively, the density and the viscosity of the fluid, k is the permeability matrix of the soil, and g the gravitational acceleration constant. Introducing the hydraulic head Φ defined by

$$(2.1) \qquad \Phi = \frac{P}{\rho_0 g} + z - h_{ref},$$

we write the previous equation as follows:

$$(2.2) \qquad q = -K\nabla\Phi - \frac{k}{\mu}(\rho - \rho_0)g e_z, \quad K = \frac{k\rho_0 g}{\mu}.$$

In this relation, the matrix K is the hydraulic conductivity which expresses the ability of the underground to conduct the fluid. We have denoted by ρ_0 the reference density of the fluid. In (2.1), $Z = z - h_{ref}$ is the elevation above a fixed datum level under the aquifer, $h_{ref} < 0$.

Next, the conservation of mass during displacement is given by the equation

$$(2.3) \qquad \partial_t(\phi\rho) + \nabla \cdot (\rho q) = \rho Q,$$

where ϕ is the porosity of the medium and Q denotes a generic source term (for production and replenishment).

2.2. State equation for the fluid compressibility. We consider that the fluids are compressible by assuming that pressure P is related to the density ρ as follows:

$$(2.4) \qquad \frac{d\rho}{\rho} = \alpha_P dP.$$

The real number $\alpha_P \geq 0$ is the fluid compressibility coefficient. We assume that fresh and salt water have the same compressibility. Further assuming $\alpha_P = 0$ we would recover the incompressible case.

2.3. State equation for the soil compressibility. The soil is a porous medium. It is a set of voids contained in a solid skeleton consisting of rock grains. We now introduce in the model the effects of the rock compressibility, that is from the possible deformations of the skeleton. This means ruling the dependence of the porosity with respect to the depth. A simple model due to Athy [5] reads

$$\phi(z) = \phi_0 e^{-Mz}, \qquad (\phi_0, M) \in \mathbb{R}_+^2.$$

Notice that no dependence of the porosity with the variation of the pressure is included in such a formula. A much more physical approach thus consists in deriving a differential equation for the porosity. First we denote by σ the total stress in the porous medium and by σ_s the stress related to the skeleton. We have

$$\sigma = \phi P + (1 - \phi)\sigma_s,$$

where term ϕP accounts for the pressure effects. From Terzaghi's theory [33], the effective stress σ_e is defined by

$$\sigma_e = (1 - \phi)(\sigma_s - P).$$

Assuming that the total stress does not change, we infer from $\sigma_e + P = \sigma$ that

$$d\sigma_e = -dP.$$

Let us now consider the variations of a given volume V of porous medium due to rock compressibility. If the grains of the porous rock are incompressible, the deformation is mainly produced by the rearrangement of the assembly of grains and the volume of the solid part $V_s = (1 - \phi)V$ remains unchanged (cf. [13]). We thus have

$$(2.5) \qquad \frac{dV_s}{d\sigma_e} = -\frac{d\phi}{d\sigma_e}V + (1 - \phi)\frac{dV}{d\sigma_e} = 0 \Leftrightarrow -\frac{1}{V}\frac{dV}{d\sigma_e} = \frac{1}{(1 - \phi)}\frac{d\phi}{dP}.$$

Assuming small volume variations and low elastic behavior for the soil justifies the definition of the soil compressibility $\beta_P \in \mathbb{R}$ by

$$\beta_P = -\frac{1}{V}\frac{dV}{d\sigma_e}.$$

Equation (2.5) then reads

$$(2.6) \qquad \beta_P = \frac{1}{1 - \phi}\frac{d\phi}{dP}.$$

2.4. Hypothesis. Let us now list the assumptions on the fluid and medium characteristics and also on the flow which are meaningful in the context of seawater intrusion in an aquifer.

2.4.1. Hypothesis on the fluid and on the medium. In the present subsection, we include the state equations presented in subsections 2.2 and 2.3 in (2.2)–(2.3) while also taking into account the specifical range of the physical parameters in an aquifer.

First, we assume that the fluids (namely, here fresh and salt water) *and* the soil are weakly compressible. It means that the densities of the fluids and the porosity of the medium weakly depend on the pressure variations, that is (in (2.4) and (2.6))

$$(2.7) \qquad\qquad \alpha_P \ll 1, \quad \beta_P \ll 1.$$

For instance, the pure water compressibility is $\alpha_P = 4.4 \times 10^{-10}$, rock compressibility is in the range $[10^{-8}, 10^{-6}]$ for clay, $[10^{-10}, 10^{-8}]$ for gravel or jointed rock (in $m^2 N^{-1}$).

Let us exploit the first assumption. In natural conditions and especially in an aquifer, one observes small fluid mobility (defined by the ratio k/μ). A first consequence of the low compressibility of the fluid combined with the low mobility of fluid appears in the momentum equation. We perform a Taylor expansion with respect to P of the density ρ in the gravity term of the Darcy equation. Neglecting the terms weighted by $\alpha_P k/\mu \ll 1$ in (2.2), we get

$$(2.8) \qquad\qquad q = -K\nabla\Phi, \quad K = \frac{k\rho_0 g}{\mu}.$$

A second consequence is $\nabla\rho \cdot q \ll 1$ which leads to the following simplification in the mass conservation equation (2.3):

$$\rho\partial_t\phi + \phi\partial_t\rho + \rho\nabla \cdot q = \rho Q.$$

Neglecting in this way the variation of density in the direction of flow is sometimes considered as an extra assumption called Bear's hypothesis (cf. [1]). Here it follows from (2.7) and separating these assumptions seems questionable. Including (2.4) and (2.6), that is $\partial_t\rho = \rho\alpha_P\partial_t P$ and $\partial_t\phi = (1-\phi)\beta_P\partial_t P$ in the latter equation, we get

$$\rho\big((1-\phi)\beta_P + \phi\alpha_P\big)\partial_t P + \rho\nabla \cdot q = \rho Q.$$

Using the hydraulic head defined in (2.1) and Darcy's law (2.8) combined with $\rho > 0$, we finally write

$$(2.9) \qquad S_0\partial_t\Phi - \nabla \cdot (K\nabla\Phi) = Q, \quad \text{where} \quad S_0 = \rho_0 g\big((1-\phi)\beta_P + \phi\alpha_P\big).$$

The fluid storage coefficient S_0 (also called storativity) characterizes the workable water volume. It accounts for the rock and fluid compressibility. In general, this coefficient is extremely small, once again due to (2.7). In what follows, we moreover assume that $S_0(\phi) \simeq S_0(P_0) \in \mathbb{R}$ (that is $\alpha_P\beta_P \simeq 0$ and $\beta_P^2 \simeq 0$ in the Taylor expansion of $S_0(P)$ near P_0).

At this point, introducing specific indicies for the fresh (f) and salt (s) waters in (2.9) and using (2.8), we have derived the following model:

$$(2.10) \qquad \begin{array}{ll} S_f\partial_t\Phi_f + \nabla \cdot q_f = Q_f, & q_f = -K_f\nabla\Phi_f, \\ S_f = \rho_f g\big((1-\phi)\beta_P + \phi\alpha_P\big), & K_f = kg\rho_f/\mu_f, \end{array}$$

$$(2.11) \qquad \begin{array}{ll} S_s\partial_t\Phi_s + \nabla \cdot q_s = Q_s, & q_s = -K_s\nabla\Phi_s, \\ S_s = \rho_s g\big((1-\phi)\beta_P + \phi\alpha_P\big), & K_s = kg\rho_s/\mu_s. \end{array}$$
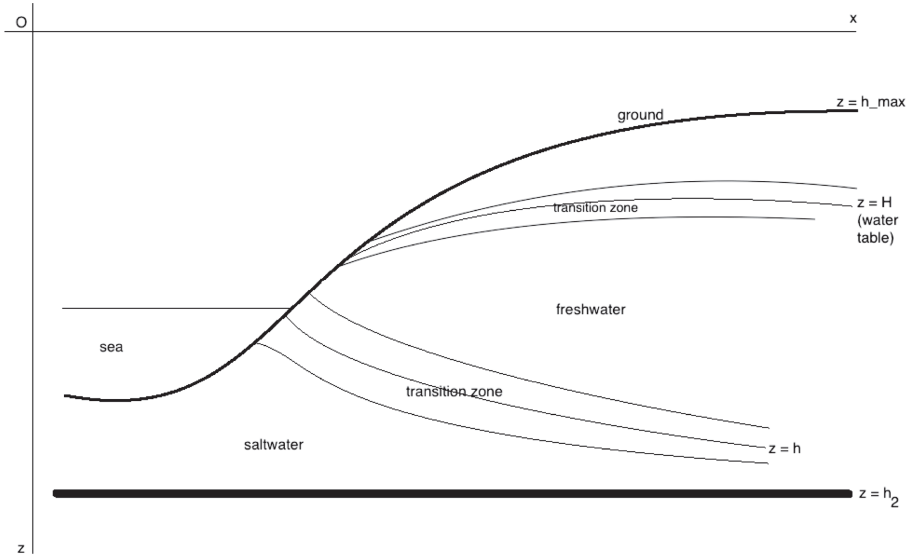
FIG. 1. *Schematic representation of saltwater intrusion in a coastal aquifer: the lower transition zone with variable salt concentration around the corresponding "virtual" sharp interface "$z = h$"; the upper transition (desaturation) zone around the corresponding "virtual" sharp interface, the water table "$z = H$."*

Remark 1. Notice that due to the difference of reference quantities $\rho_f \neq \rho_s$, the model is density driven. The approach is however different from Muskat's where density variations in the flow direction "$\nabla \rho \cdot q$" are not neglected and where (2.9) is thus replaced by: $\rho S_0 \partial_t \Phi - \nabla \cdot (\rho K \nabla \Phi) = \rho Q$.

2.4.2. Hypothesis on the flow. The following two assumptions are introduced for upscaling the 3D problem to a 2D model in the next subsection.

Sharp interfaces. The slow dynamics of the displacement in the aquifer let the fluids tend to the picture described in Figure 1. Of course, freshwater and saltwater are miscible. Therefore they are separated by a transition zone characterized by the variations of the salt concentration. Nevertheless the thickness of the transition zone is small compared to dimensions of the aquifer. We then assume that an abrupt interface separates two distinct domains, one for the saltwater and one for the freshwater. A sharp interface is also assumed to separate the saturated and the dry parts of the aquifer, thus neglecting the thickness of the partially saturated zone. This latter free interface may be viewed as a moving water table. This approximation is justified because the thickness of the capillarity fringe is much smaller than the distance to the ground surface. We will alleviate these assumptions by reincluding somehow mass transfers around interfaces in subsection 2.6 below.

Notice moreover that the slow dynamics of the displacement and the gravity effects (here the lighter fluid is above the heavier fluid) allow us to assume that both the interfaces are graphs.

Dupuit approximation (hydrostatic approach). The Dupuit assumption supposes that [8] the hydraulic head is constant along each vertical direction (vertical equipotentials). It is legitimate since one actually observes quasi-horizontal displacements when the thickness of the aquifer is small compared to its width and its length and when the flow is far from sinks and wells. This approximation is exact in the case of a homogeneous, isotropic, and confined aquifer with constant thickness.

2.5. Upscaling procedure. We now use the approximations introduced in 2.4.2 to vertically integrate (2.10)–(2.11), thus reducing the 3D problem to a 2D problem.

2.5.1. Vertical integration. The aquifer is represented by a 3D domain $\Omega \times (h_2, h_{\max})$, $\Omega \subset \mathbb{R}^2$, function h_2 (resp., $h_{\max}$) describing its lower (resp., upper) topography. For the sake of simplicity, we assume that the upper surface of the aquifer is at constant depth, $h_{\max} \in \mathbb{R}$, and moreover that $h_{\max} = 0$.

We denote by H (resp., h) the depth of the free interface separating the freshwater layer and the dry part of the aquifer (resp., the saltwater layer). Since we do not consider very deep geologic formations, we assume that the pressure is constant and equal to the atmospheric pressure P_a in the upper dry part of the aquifer, that is between $z = H$ and $z = 0$. We impose pressure equilibrium at the boundary of each area, more precisely,

$$
(2.12) \qquad
\begin{cases}
\text{If } H < h_{\max} = 0: & \Phi_{f|z=H} = P_a/\rho_f g + H - h_{ref}, \\
\text{If } H = h_{\max} = 0: & \Phi_{f|z=h_{\max}} = P_a/\rho_f g - h_{ref}.
\end{cases}
$$

It follows that the right quantity for the hydraulic head Φ_f to be meaningful in the whole aquifer is $H^- = \inf(0, H)$. The upper head equilibrium condition (2.12) reads $\Phi_{f|z=H^-} = P_a/\rho_f g + H^- - h_{ref}$. Similar elements on the depth of the salt interface h lead us to introduce $h^- = \inf(0, h)$.

Now we perform the vertical integration. We begin with the freshwater zone between depths h^- and H^-. We obtain

$$
\int_{h^-}^{H^-} \left(S_f \partial_t \Phi_f + \nabla \cdot q_f \right) dz = \int_{h^-}^{H^-} Q_f \, dz, \quad B_f = H^- - h^-.
$$

Applying the Leibnitz rule to the first term in the left-hand side yields

$$
\int_{h^-}^{H^-} S_f \partial_t \Phi_f dz = S_f \frac{\partial}{\partial t} \int_{h^-}^{H^-} \Phi_f dz + S_f \Phi_{f|z=h^-} \partial_t h^- - S_f \Phi_{f|z=H^-} \partial_t H^-.
$$

We denote by $\tilde{\Phi}_f$ the vertically averaged hydraulic head

$$
\tilde{\Phi}_f = \frac{1}{B_f} \int_{h^-}^{H^-} \Phi_f dz.
$$

Because of the Dupuit approximation, $\Phi_f(x_1, x_2, z) \simeq \tilde{\Phi}_f(x_1, x_2)$, $x = (x_1, x_2) \in \Omega$, $z \in (h^-, H^-)$, we have

$$
\int_{h^-}^{H^-} S_f \partial_t \Phi_f dz = S_f B_f \partial_t \tilde{\Phi}_f.
$$

We also have

$$
\int_{h^-}^{H^-} \nabla \cdot q_f \, dz = \nabla' \cdot (B_f \tilde{q}'_f) + q_{f|z=h_1^-} \cdot (e_z - \nabla H^-) - q_{f|z=h^-} \cdot (e_z - \nabla h^-),
$$

where $\nabla' = (\partial_{x_1}, \partial_{x_2})$, $q'_f = (q_{f,x_1}, q_{f,x_2})$, and the averaged Darcy velocity $\tilde{q}'_f = \frac{1}{B_f} \int_{h^-}^{H^-} q'_f \, dz$ is given by

$$
\tilde{q}'_f = -\frac{1}{B_f} \int_{h^-}^{H^-} \left(K'_f \nabla' \Phi_f \right) dz = -\frac{1}{B_f} \int_{h^-}^{H^-} \left(K'_f \nabla' \tilde{\Phi}_f \right) dz = -\tilde{K}'_f \nabla' \tilde{\Phi}_f,
$$

$$
\tilde{K}'_f = \frac{1}{B_f} \int_{h^-}^{H^-} K'_f \, dz.
$$

We denote by $\tilde{Q}_f$ the source term representing distributed surface supply of fresh water into the free aquifer:

$$\tilde{Q}_f = \frac{1}{B_f} \int_{h^-}^{H^-} Q_f \, dz.$$

The averaged mass conservation law for the freshwater thus finally reads

$$S_f B_f \partial_t \tilde{\Phi}_f = \nabla' \cdot (B_f \tilde{K}'_f \nabla' \tilde{\Phi}_f) - q_{f|z=H^-} \cdot (e_z - \nabla H^-)$$

(2.13)
$$+ q_{f|z=h^-} \cdot (e_z - \nabla h^-) + B_f \tilde{Q}_f.$$

Similar computations in the saltwater layer give

$$S_s B_s \partial_t \tilde{\Phi}_s = \nabla' \cdot (B_s \tilde{K}'_s \nabla' \tilde{\Phi}_s) + q_{s|z=h_2} \cdot (e_z - \nabla h_2)$$

(2.14)
$$- q_{s|z=h^-} \cdot (e_z - \nabla h^-) + B_s \tilde{Q}_s,$$

where $B_s = h^- - h_2$ is the thickness of the saltwater zone. In these equations, the term $B_i \tilde{K}'_i$, $i = f, s$, may be viewed as the dynamic transmissivity of each layer. At this point, we have obtained an underdetermined system of two PDEs (2.13)–(2.14) with four unknowns, $\tilde{\Phi}_i$, $i = f, s$, H^-, and h^-.

2.6. Fluxes and continuity equations across the interfaces. Our aim is now to include in the model the continuity and transfer properties across interfaces. As a consequence, we express the four flux terms appearing in (2.13)–(2.14) and we reduce the number of unknowns, the remaining ones being the interfaces height functions.

2.6.1. Fluxes across the interfaces. The present subsection is fundamental. Indeed our approach began like a sharp interface approach: we have averaged the equations in the vertical direction between the bottom of the aquifer and two interfaces; as already mentioned, these interfaces are virtual since they actually approximate two thin transition zones, the mixing layer where salt and fresh water coexist and the desaturation layer (see Figure 1). Now we reinclude existence of these two layers in the model in the form of two diffuse interfaces: one of characteristic thickness δ_H between the dry and saturated zones and the other one of characteristic thickness δ_h between fresh and salt water. As mentioned in the introduction, this coupled sharp-diffuse interface approach is the new point relative to the existing literature that makes our work completely original. The dynamics of these diffuse interfaces is ruled by phase-field models.

Phase-field models were first introduced for the description of phase transitions and solidification processes [11]. They are now largely used for modeling binary fluids transitions. Closer to our context, such models are employed to describe imbibition in porous media [16] (comparable to the upper interface in our setting). In phase separation problems the model typically contains a double-well potential in which the local minima correspond to the homogeneous stable states. Here we rather use a triple-well potential for respecting the primal sharp interface approach and for including the effect of this macroscopic front in the local phase-field model. The energy functional also contains nonlocal terms involving the gradient (and possibly higher order derivatives) of the phase field. In the present work we choose a simple model, namely, based on a tristable Allen–Cahn-type model (see, e.g., [27]). As already mentioned the fact that the Allen–Cahn model, contrary to the Cahn–Hilliard's one, is

characterized by nonconserved fields (see [22]) will not impact the conservative form of our final model. The nondegenerate mobility choice for the phase-field model is also well-based in terms of the physics because occurence of pure phases and thus of vanishing mobility does not make sense in our miscible context, contrary to the context of phase separation.

• **Flux across the fresh-saltwater interface** We introduce an order parameter F_h (the phase field) that "labels" the two "phases" (salt and fresh water) and the sharp interface:

$$F_h = \begin{cases} 0 & \text{in freshwater,} \\ c_s/2 & \text{on sharp interface,} \\ c_s & \text{in saltwater,} \end{cases}$$

where c_s is, e.g., the mean concentration of salt in the salty area. Indeed we choose to define the virtual interface by isosurface $c_s/2$. The sharp interface at time t corresponds to set $\left\{ (x, z) = (x_1, x_2, z) \text{ s.t. } F_h(x, z, t) = c_s/2 \right\}$. The function F_h satisfies a modified Allen–Cahn equation with three points of stability,

$$(2.15) \qquad \partial_t F_h + \vec{v} \cdot \nabla F_h - \delta_h \Delta' F_h + \frac{2F_h(F_h - c_s/2)(F_h - c_s)(3F_h^2 - c_s^2/4)}{\delta_h} = 0.$$

The detailed shape of the triple-well potential is not important; its main role is to establish and maintain well-defined domain walls. The elastic relaxation built into the phase-field dynamics prevents the interfacial mixing layer from spreading out. This point corresponds to the observations in the aquifers considered in the present paper. The characteristic size of the corresponding diffuse interface is $\delta_h > 0$ (see, e.g., [3] for rigorous results). The parameter δ_h is small. Another point in the favor of the coupling of (2.15) with the sharp interface approach is indeed the convergence as $\delta_h \to 0$ of the phase-field model to a sharp interface one (see [26] for Allen–Cahn, [12, 9] for Cahn–Hilliard and Stefan, and Remark 2). The phase-field equation (2.15) also contains advection of the order parameter by the fluid, the effective velocity being denoted by $\vec{v}$ [10]. Note that we have already neglected here the vertical diffusion with regard to the convective term.

Since the stability set $\{F_h = c_s/2\}$ corresponds to the sharp interface of depth h^-, we have

$$F_h(x, z, t) = c_s/2 \iff z - h^-(x, t) = 0.$$

The derivative of the constant function $F_h(x, h^-(x, t), t) = c_s/2$ is null. We infer from $\partial_i[F_h(x, h^-(x, t), t)] = 0$, $i = x, t$, that $\partial_t F_h(x, h^-, t) = -\partial_z F_h(x, h^-, t)\partial_t h^-$ and $\nabla' F_h(x, h^-, t) = -\partial_z F_h(x, h^-, t)\nabla' h^-$. Deriving once again the latter relation we compute $\Delta' F_h(x, h^-, t) = -\partial_z F_h(x, h^-, t)\Delta' h^- - \partial_{zz}^2 F_h(x, h^-, t)|\nabla' h^-|^2 - \nabla' \partial_z F_h(x, h^-, t) \cdot \nabla' h^-$. Including these results in the projection of the Allen–Cahn equation for $F_h = c_s/2$, we get

$$\partial_z F_h\left(-\partial_t h^- + \vec{v} \cdot (e_z - \nabla h^-) + \delta_h \Delta' h^-\right) + \delta_h \nabla' h^- \cdot \nabla' \partial_z F_h + \delta_h |\nabla' h^-|^2 \partial_{zz}^2 F_h = 0.$$

The two last terms of the left-hand side of the latter relation may be neglected. Indeed they combine three low order quantities. First, of course, the diffusion parameter δ_h which is the characteristic size of the diffuse interface is small. Next point comes from the dynamics of the Allen–Cahn equation. A formal asymptotic analysis shows that the reaction term is dominant at small times, so that in the rescaled

time scale $t' = t/\delta_h^2$ the dynamics essentially lie in the ODE $\partial_{t'} F_h = 2F_h(F_h - c_s/2)$ $(F_h - c_s)(3F_h^2 - c_s^2/4)$ and the values of F_h tend to the stable values thus creating steep transition layers. Then the propagation is associated with a much slower time scale, convective and diffusive terms coming to balance with the reaction term near the stable surfaces, but the regular steep structure of the diffuse interface ensures small $\nabla' \partial_z F_h$ and order one $\partial_{zz}^2 F_h$. Furthermore Dupuit's work [17] is based on the observation that in such a groundwater flow the slope of the interfacial surface is very small, that is, $|\nabla' h^-| \ll 1$. For the same reason, the function F_h heuristically behaves like a step function in the vertical direction and $\partial_z F_h \neq 0$. The latter equation thus gives

$$(2.16) \qquad -\partial_t h^- + \vec{v} \cdot (e_z - \nabla h^-) + \delta_h \Delta' h^- = 0.$$

We then turn back to the traditional sharp interface characterization. Actually it turns out that the velocity $\vec{v}$ in the mixing zone which transports the interface in (2.15) and which seems to be an additional unknown in the model disappears at this stage. We thus do not have to introduce a supplementary equation for closing the system (as for instance in [29]). There is no mass transfer across the interface between fresh and salt water, i.e., the normal component of the effective velocity is continuous at the interface $z = h^-$:

$$(2.17) \qquad \left(\frac{q_{f|z=h^-}}{\phi} - \vec{v} \right) \cdot \vec{n} = \left(\frac{q_{s|z=h^-}}{\phi} - \vec{v} \right) \cdot \vec{n} = 0,$$

where $\vec{n}$ denotes the normal unit vector to the interface, $\vec{n} = |\nabla(z - h^-)|^{-1} \nabla(z - h^-)$.

Combining (2.16) and (2.17), we obtain

$$q_{f|z=h^-} \cdot (e_z - \nabla h^-) = q_{s|z=h^-} \cdot (e_z - \nabla h^-) = \phi(\partial_t h^- - \delta_h \Delta' h^-)$$
$$(2.18) \qquad = \phi\big(\mathcal{X}_0(-h)\partial_t h - \delta_h \nabla' \cdot (\mathcal{X}_0(-h)\nabla' h)\big)$$

where we set

$$\mathcal{X}_0(h) = \begin{cases} 0 & \text{if} \quad h \leq 0, \\ 1 & \text{if} \quad h > 0. \end{cases}$$

Relation (2.18) is a regularized Stefan-type boundary condition.

Remark 2. For emphasizing once again the consistency with our primal sharp interface approach, we recall that rigorous asymptotic results let us recover the sharp interface evolution equation. More precisely, if $\delta_h \to 0$, the Allen–Cahn model tends to the classical Stefan problem, that is the classical modeling of the interface evolution given by a level-set equation $q_f(h^-) \cdot (e_z - \nabla h^-) = \phi \partial_t h^-$ (see [24]). If the Allen–Cahn equation (here in the case of one point of stability) is written as

$$\partial_t F^\epsilon + \vec{v} \cdot \nabla F^\epsilon - \gamma \Delta F^\epsilon + \frac{F^\epsilon(F^\epsilon - c_s/2)(F^\epsilon - c_s)}{\epsilon \delta_h} = 0,$$

γ being a parameter related to the elasticity of the interface and to δ_h, when letting $\epsilon \to 0$ for any given γ, we get (see [2] and the references therein)

$$\partial_t F + \vec{v} \cdot \nabla F - \gamma \Delta F = 0.$$

● **Flux across the unsaturated-saturated interface** We perform the same reasoning for the upper capillary fringe. Likewise, defining the phase function F_1 by

$$F_1 = \begin{cases} -1 & \text{in} \quad \text{unsaturated} \quad \text{zone}, \\ 0 & \text{at} \quad \text{sharp} \quad \text{interface}, \\ 1 & \text{in} \quad \text{saturated} \quad \text{zone}, \end{cases}$$

the sharp interface is characterized by $F_1(x, z, t) = 0 \iff z - H^-(x,t) = 0$. The leading order terms of the projection on $z = H^-$ of a tristable Allen–Cahn equation for a diffuse interface of characteristic size δ_H give

$$(2.19) \qquad -\partial_t H^- + \vec{v}_1 \cdot (e_z - \nabla H^-) + \delta_H \Delta' H^- = 0.$$

We combine the latter equation with the relation ruling continuity of the normal component of the velocity

$$\left(\frac{q_{f|z=H^-}}{\phi} - \vec{v}_1 \right) \cdot \vec{n} = 0,$$

and we obtain

$$
\begin{aligned}
q_{f|z=H^-} \cdot (e_z - \nabla H^-) &= \phi\big(\partial_t H^- - \delta_H \Delta' H^-\big) \\
&= \phi\big(\mathcal{X}_0(-H)\partial_t H - \delta_H \nabla' \cdot \big(\mathcal{X}_0(-H)\nabla' H\big)\big).
\end{aligned}
$$
$$(2.20)$$

• **Impermeable layer at $z = h_2$** If the lower layer is impermeable, there is no flux across the boundary $z = h_2$:

$$(2.21) \qquad q_s(h_2) \cdot (e_z - \nabla h_2) = 0.$$

2.6.2. Continuity equations. Continuity relations now imposed on the interfaces will allow us to properly reduce the number of unknowns in (2.13)–(2.14).

The Dupuit approximation reads $\tilde{\Phi}_f \simeq \Phi_{f|z=H^-}$, that is,

$$(2.22) \qquad \tilde{\Phi}_f = \frac{P_a}{\rho_f g} + H^- - h_{ref}.$$

Bearing in mind the boundary condition (2.12) at the upper free interface and approximation $\Phi_{f|z=H^-} \simeq \Phi_{f|z=h^-}$, we have

$$\frac{P_a}{\rho_f g} + H^- - h_{ref} = \frac{P_{f|z=h^-}}{\rho_f g} + h^- - h_{ref} \iff P_{f|z=h^-} = P_a + \rho_f g(H^- - h^-).$$

Besides, the pressure is continuous at the interface between salt and fresh water. Since $P_{s|z=h^-} = \rho_s g(\Phi_{s|z=h^-} - h^- + h_{ref})$ and $\Phi_{s|z=h^-} \simeq \tilde{\Phi}_s$, it follows that

$$(2.23) \qquad (1+\alpha)\tilde{\Phi}_s = \frac{P_a}{\rho_f g} + H^- + \alpha h^- - (1+\alpha)h_{ref}, \quad \alpha = \frac{\rho_s}{\rho_f} - 1.$$

Parameter α characterizes the density contrast.

Equations (2.22)–(2.23) allow us to eliminate $\tilde{\Phi}_f$ and $\tilde{\Phi}_s$ in the final system.

2.6.3. Presence of other water ressources. Up to now, we have considered that the aquifer is surrounded by a dry zone. Other settings may of course be included in the model and may impact (2.20)–(2.21). We mention two important cases in the present subsection although we do not numerically illustrate them in the present paper.

Presence of free water (river...) in a part of the upper boundary may be treated by prescribing the continuity of the hydraulic head. Assume existence of a deflection in a part $\Omega_r \times \{0\}$, $\Omega_r \subset \Omega$, of the upper bound of the aquifer containing a river of

depth $|h_{riv}|$. The river is in hydrodynamic equilibrium with the atmosphere, that is, if P_r is the pressure in the river,

$$P_r(x_1, x_2, z) = P_a + \rho_f g(0 - z), \ (x_1, x_2) \in \Omega_r, \ h_{riv} \leq z \leq 0.$$

The hydraulic head of the river Φ_r is thus also constant with regard to z, just like Φ_f. The usual boundary condition at the interface between the aquifer and the river consists in prescribing the continuity of the hydraulic head. It reads

$$\Phi_{f|\{x\in\Omega_r,\, z=h_{riv}\}} = \Phi_{r|\{x\in\Omega_r,\, z=h_{riv}\}} = \frac{P_{r|z=h_{riv}}}{\rho_f g} + h_{riv} - h_{ref} = \frac{P_a}{\rho_f g} - h_{ref}.$$

Bearing in mind the general definition of $\tilde{\Phi}_f$ in the aquifer (see (2.22)), we can interpret the latter relation: when the free water interface touches the river, the model includes the river depth in the freshwater zone and H^- jumps from h_{riv} to 0. In this case, the flux term is $q_{f|z=H^-=h_{riv}} \cdot (e_z - \nabla H^-) = 0$. The same type of boundary condition holds true along the outflow face for freshwater along the bottom of the sea (with of course a term containing the density ratio ρ_s/ρ_f instead of $1/\rho_f$; see [8, section 9.7]). But in this case, the Dupuit assumption fails.

Another possibility is the presence of a weakly impermeable zone (aquitard). Flux between the aquitard and the water contained in the aquifer consists of a leakage term q_L. The generic model for recharge and discharge is $q_L = (\Phi_{ext} - \Phi)/c_m$, where Φ (resp., Φ_{ext}) is the head on the aquifer's (resp., aquitard's) side of the semipermeable "membrane," resistance $c_m = \mathcal{O}(b_m/k_m)$ depending on the thickness b_m and on the permeability k_m ($k_m \ll k$) of the membrane (see, e.g., [30]). This formulation allows us to treat charge and discharge, depending on the ratio between Φ and Φ_{ext}. Here we can include a fresh leakage term q_{Lf} from the top of the aquifer to the fresh water when the aquifer is fully saturated (that is $H = 0$) and a salty leakage term q_{Ls} from the bottom to the saltwater:

$$(2.24) \quad q_{f|z=H^-} \cdot (e_z - \nabla h_1^-) = q_{Lf} \text{ when } H^- = 0, \quad q_{s|z=h_2} \cdot (e_z - \nabla h_2) = -q_{Ls}.$$

More precisely, in view of (2.22), term q_{Lf} reads

$$q_{Lf}(x, H, h)$$
$$= \left(1 - \chi_0(-H)\right)\chi_0(H^- - h^-)\frac{k_{mf}(x)}{b_{mf}(x)}\left(\frac{P_{ext,f}(x)}{\rho_f g} + b_{mf}(x) - \frac{P_a}{\rho_f g} - H^-\right)$$
$$= \left(1 - \chi_0(-H)\right)\chi_0(H^- - h^-)\frac{k_{mf}(x)}{b_{mf}(x)}\left(\frac{P_{ext,f}(x)}{\rho_f g} + b_{mf}(x) - \frac{P_a}{\rho_f g}\right).$$

Indeed we specify that only fresh exchanges are allowed, thus the term $\chi_0(H^- - h^-)$, and that the semipermeable zone is at depth $h_{\max} = 0$, thus the term $(1 - \chi_0(-H))$ (we consider here a phreatic aquifer: there is no leakage at the upper boundary unless the aquifer is fully saturated). We impose $k_{mf} = 0$ outside the aquitard's area. The same type of arguments and (2.23) lead to

$$q_{Ls}(x, H, h)$$
$$= \chi_0(h^- - h_2)\frac{k_{ms}(x)}{b_{ms}(x)}\left(\frac{P_{ext,s}(x)}{\rho_s g} + h_2 - b_{ms}(x) - \frac{P_a}{\rho_f g(1+\alpha)} - \frac{H^-}{1+\alpha} - \frac{\alpha h^-}{1+\alpha}\right).$$

2.7. Conclusion: seawater intrusion model. We begin by some assumptions, essentially introduced for the sake of simplicity of the equations. The medium is supposed to be isotropic and the viscosity the same for the salt and fresh water. Using definition (2.2) for the permeabilities $\tilde{K}'_f$ and $\tilde{K}'_s$, it follows from $\mu_f = \mu_s$ that

$$(2.25) \qquad\qquad \tilde{K}'_s = (1+\alpha)\tilde{K}'_f.$$

The 2D model (2.13)–(2.14) now reads

$$
\begin{aligned}
& S_f B_f \partial_t \tilde{\Phi}_f - \nabla' \cdot (B_f \tilde{K}'_f \nabla' \tilde{\Phi}_f) + q_{f|z=H^-} \cdot (e_z - \nabla H^-) \\
(2.26) &\qquad\qquad - q_{f|z=h^-} \cdot (e_z - \nabla h^-) = B_f \tilde{Q}_f, \\
& S_s B_s \partial_t \tilde{\Phi}_s - (1+\alpha)\nabla' \cdot (B_s \tilde{K}'_f \nabla' \tilde{\Phi}_s) - q_{s|z=h_2} \cdot (e_z - \nabla h_2) \\
(2.27) &\qquad\qquad + q_{s|z=h^-} \cdot (e_z - \nabla h^-) = B_s \tilde{Q}_s.
\end{aligned}
$$

We can neglect the term $S_s B_s \partial_t \tilde{\Phi}_s$ because of the two following arguments. First the saltwater is confined since the bottom of the aquifer is assumed essentially impermeable:

$$\partial_t \Phi_s \ll 1.$$

Besides $S_s \ll 1$ because of the weak compressibility of the fluid and of the rock (see (2.7)), hence

$$S_s = \rho_s g\big((1-\phi)\beta_P + \phi\alpha_P\big) \ll 1.$$

We now choose to base the model on the salt mass conservation and on the total mass conservation. We thus write (2.27) using $S_s B_s \partial_t \tilde{\Phi}_s \simeq 0$, and the sum of (2.26) and (2.27):

$$
\begin{aligned}
& -(1+\alpha)\nabla' \cdot \big(B_s \tilde{K}'_f \nabla' \tilde{\Phi}_s\big) + q_{s|z=h^-} \cdot \nabla\big(z-h^-\big) - q_{s|z=h_2} \cdot \nabla\big(z-h_2\big) = B_s \tilde{Q}_s, \\
& S_f B_f \partial_t \tilde{\Phi}_f - \nabla' \cdot \big(B_f \tilde{K}'_f \nabla' \tilde{\Phi}_f\big) - (1+\alpha)\nabla' \cdot \big(B_s \tilde{K}'_f \nabla \tilde{\Phi}_s\big) + q_{f|z=H^-} \cdot \nabla\big(z-H^-\big) \\
& \qquad\qquad - q_{s|z=h_2} \cdot \nabla\big(z-h_2\big) = B_f \tilde{Q}_f + B_s \tilde{Q}_s.
\end{aligned}
$$

Once again for the sake of simplicity, we assume $\delta_h = \delta_H := \delta$ (the diffuse interfaces widths are of the same order). We have no need for truncations involving χ_0, since a maximum principle has been established for the previous model in [14]. Bearing in mind that now $B_s = h^- - h_2$, $B_f = H^- - h^-$, and using (2.18), (2.20), (2.21), and (2.22)–(2.23), we write the latter system as

$$
(\mathcal{M}) \quad
\begin{cases}
\phi \partial_t h - \nabla' \cdot \big(\alpha \tilde{K}'_f (h - h_2)\nabla' h\big) - \nabla' \cdot \big(\delta\phi\nabla' h\big) \\
\qquad - \nabla' \cdot \big(\tilde{K}'_f (h_2 - h)\nabla' H\big) - q_{Ls}(x, H, h) = \tilde{Q}_s(h - h_2), \\
\big(S_f(H - h) + \phi\big)\partial_t H - \nabla' \cdot \big(\tilde{K}'_f\big((H - h) + (h - h_2)\big)\nabla' H\big) \\
\qquad - \nabla' \cdot \big(\delta\phi\tilde{K}'_f\nabla' H\big) - \nabla' \cdot \big(\tilde{K}'_f\alpha(h - h_2)\nabla' h\big) \\
\qquad - q_{Lf}(x, H, h) - q_{Ls}(x, H, h) = \tilde{Q}_f(H - h) + \tilde{Q}_s(h - h_2).
\end{cases}
$$

Leakage terms q_{Lf} and q_{Ls} are defined after (2.24). This system gives a 2D description

	Porosity	Permeability	Storativity	Diffuse interface depth
	ϕ	$\tilde{K}'_f$ (m/day)	S_f	δ (m)
Fig. 4	0.3	39.024	0	0 and 0.1
Figs. 5–6	0.3	39.024	0 and 0.25	0.1
Fig. 7	0.3	304.48	0	space dependent and $\delta = 0.1$
Figs. 8–11	0.35	304.48	0	0 and $\mathcal{O}(1)$ given by [15]
Fig. 9	0.35	304.48	0	0
Fig. 10	0.35	304.48	0	$\mathcal{O}(1)$ given by [15]

FIG. 2. *Parameters used in the simulations.*

for tracking a saltwater front in a free aquifer, the third dimension remaining in the model thanks to the unknowns h and H which are the free interfaces depths.

3. Numerical simulations. The present section is devoted to numerical illustrations of the behavior of the model derived above. The discretization is based on finite elements in space and on a semi-implicit Euler method in time. Let us briefly sketch the scheme.

We use a semi-implicit in time scheme combined with a $P1$ finite element method to discretize our problem. More precisely, we use the following numerical scheme:

$$
\begin{cases}
\phi \dfrac{h^{n+1} - h^n}{dt} - \nabla' \cdot \left(\alpha \tilde{K}'_f (h^n - h_2) \nabla' h^{n+1} \right) - \nabla' \cdot \left(\delta \phi \nabla' h^{n+1} \right) \\
\qquad - \nabla' \cdot \left(\tilde{K}'_f (h_2 - h^{n+1}) \nabla' H^n \right) = \tilde{Q}_s (h^{n+1} - h_2), \\[2mm]
\left(S_f (H^n - h^n) + \phi \right) \dfrac{H^{n+1} - H^n}{dt} - \nabla' \cdot \left(\tilde{K}'_f \big((H^n - h^n) + (h^n - h_2) \big) \nabla' H^{n+1} \right) \\
\qquad - \nabla' \cdot \left(\delta \phi \tilde{K}'_f \nabla' H^{n+1} \right) - \nabla' \cdot \left(\tilde{K}'_f \alpha (h^{n+1} - h_2) \nabla' h^{n+1} \right) \\
\qquad = \tilde{Q}_f (H^{n+1} - h^{n+1}) + \tilde{Q}_s (h^{n+1} - h_2).
\end{cases}
$$

This choice leads to a condition of CFL type between the time step and space discretization (the condition remains reasonable; for instance, δ_t is of order 0.5 while $\delta_x = O(1)$ for the computations of Figure 7, δ_t is of order 0.01, while $\delta_x = O(1)$ for those of Figure 8). We adapt to our case the package FreeFem++ by Pironneau and coworkers. The reader is referred to [23] for details about it.

The aquifer is figurated by a parallelepiped $(x, y) \in [-50, 50] \times [-20, 20]$, $z \in [-10, 0]$. The physical parameters have been chosen in agreement with [8]. In the following simulations, we solve numerically the full bidimensional problem and we plot the cross-sectional (at $y = 0$) elevations h and H of the virtual interfaces. The choice $y = 0$ is arbitrary since the problem is 2D. The physical parameters used in the simulations are given in Figure 2. The exterior factors affecting the dynamics in the aquifer are also summarized in Figure 3. For all the simulations, we have used homogeneous Neumann boundary conditions at the right boundary of the domain to let the interfaces freely evolve.

We first mention that our model with small δ has first been compared with results obtained by the purely sharp interface approach in [21]. Since this reference contains comparisons with well-known test problems already published, the complete similarity with our results validates our model in the case of a thin mixing zone (see Figure 4). Let us also emphasize that we benefit here from the maximum principle satisfied by the solutions of our model. Actually (see [14]) the solutions of model $(\mathcal{M})$ are

	Source term	Left boundary condition for h	Left boundary condition for H
Fig. 4	injection well	homogeneous Neumann	homogeneous Neumann
Fig. 5	injection well	homogeneous Neumann	homogeneous Neumann
Fig. 6	pumping well	homogeneous Neumann	homogeneous Neumann
Fig. 7	no	homogeneous Neumann	homogeneous Neumann
Figs. 8–11	no	oscillating Dirichlet	homogeneous Neumann
Figs. 9–10	no	oscillating Dirichlet	homogeneous Neumann and oscillating Dirichlet

FIG. 3. *Exterior factors used in the numerical tests.*
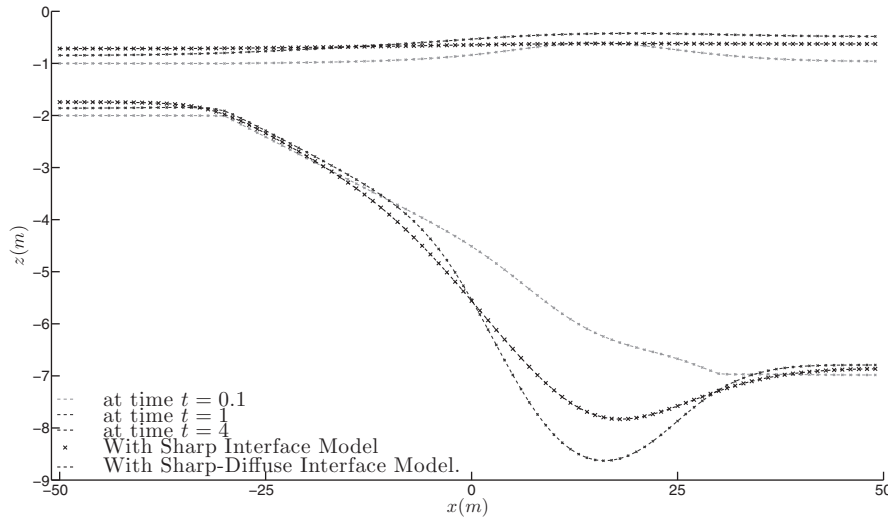
FIG. 4. *Agreement between our model with small δ (here $\delta = 0.1\,m$) and the classical sharp interface approach inspired by* [21]. *A large quantity of fresh water is injected during a short time (0.8 day) through a well of radius 1 m centered at $(x, y) = (15, 0)$. The lower interface h between salt and fresh water and the upper interface H between saturated and unsaturated zones then freely evolve. Results at times $t = 0.1$, 1, 4 days. The dash curves and the cross curves agree.*

such that $h_2 \leq h \leq H \leq 0$. We have observed that the same property is satisfied by our numerical solutions (even if our numerical method may or may not obey the same maximum principle). It follows that we do not have to truncate the numerical solutions as in [21].

The next figures are devoted to phenomenological aspects of the potential compressibility of the soil. Storativity is characterized by parameter S_f. Intuitively, the bigger S_f is, the more water may be contained in the soil. Existing upscaled models use assumption (2.7) for neglecting the storage coefficient S_f. Figure 5 corresponds to an injection *scenario*. Since the compressible soil ($S_f \neq 0$) may contain more water, we observe an overestimate of the water-table height and an underestimate of the salt interface height when considering $S_f = 0$. These misestimates subsist more than three days after the end of the injection (then the misestimates reverse). Such an injection process is classically used by operators for bringing down the salty interface. Neglecting S_f produces an overestimation of the impact of the process, especially in the injection zone. Figure 6 exhibits opposite under/over estimates during a pumping *scenario*. We also observe a local depression of the water table and apparition of a salty cone.
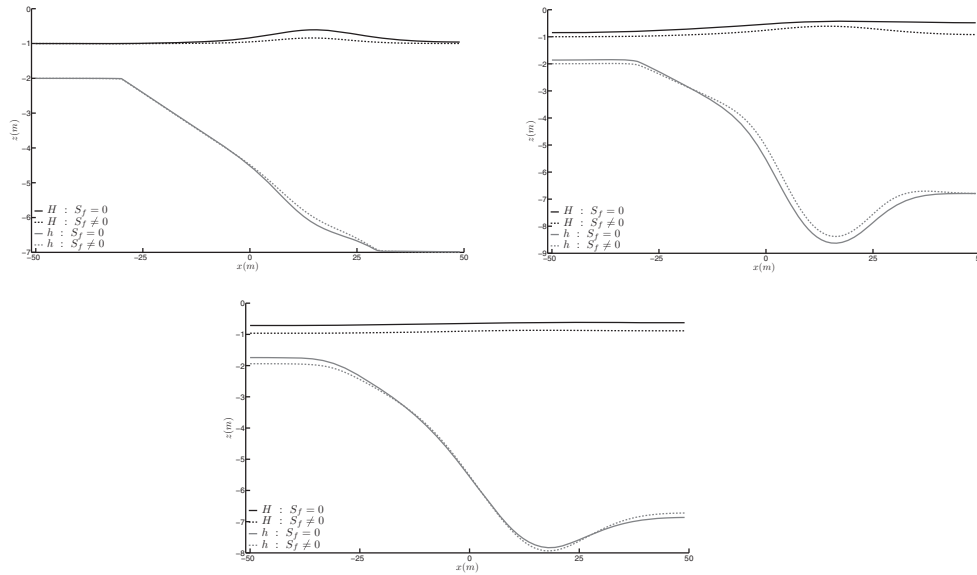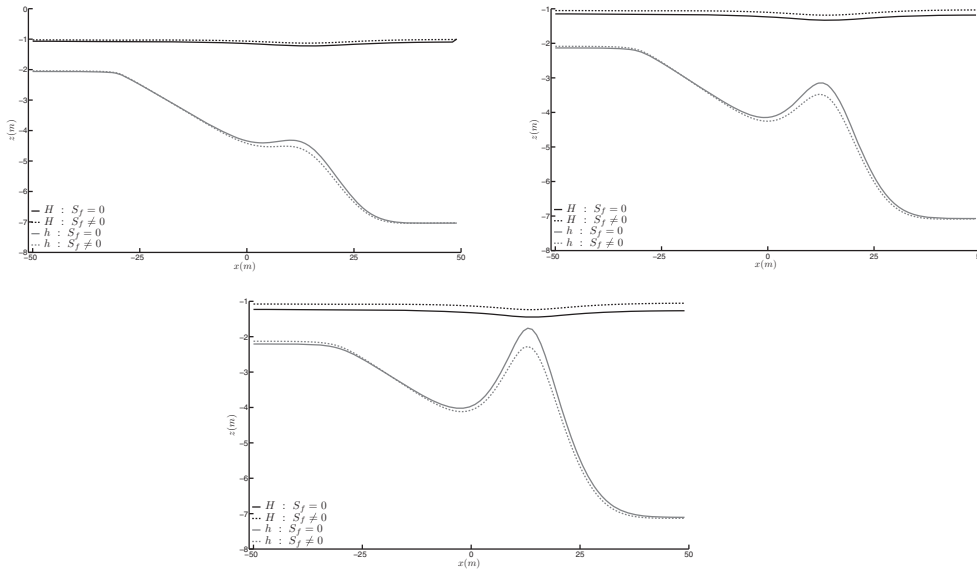
Fig. 5. *Comparison of the interfaces depth h and H in a compressible soil (dotted lines,*
$S_f = 0.25 \neq 0$*) and in an incompressible soil* ($S_f = 0$) *during an injection* scenario. *Injection and
data are the same as in Figure* 4. *Sequence of results at times* $t = 0.1$, 1, 4 *days (left to right, top
to bottom).*

Fig. 6. *Comparison of the interfaces depth h and H in a compressible soil (dotted lines,*
$S_f = 0.25 \neq 0$*) and in an incompressible soil* ($S_f = 0$) *during a pumping* scenario. *Pumping is
constant in time through a well of radius* 1 *m centered at* $(x, y) = (15, 0)$. *Sequence of results at
times* $t = 1$, 2, 3 *days (left to right, top to bottom).*

Let us now leave the comfort zone of thin mixing zones. As noticed for instance in
[15], in such a case dispersion produces nonnegligible effects: it creates head losses that
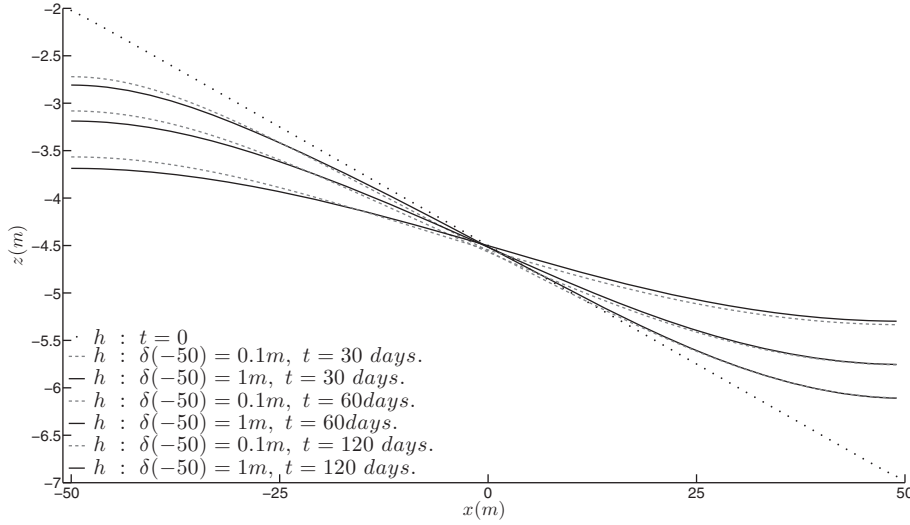lessen the area of the aquifer occupied by saltwater. Indeed salty water discharges

FIG. 7. *Effect of the characteristic width of the diffusion/mixing area: focus on the lowering of the saltwater front depth h due to mixing. Parameters are those of [15]. The mixing zone being thicker on the side of the shoreline, we test with $\delta(x) = \chi_{(-50,-20)}(x) + 0.1\,\chi_{(10,50)}(x) + (0.4 - 0.03\,x)\chi_{(-20,10)}(x)$ (case $\delta(-50) = 1$). The result is compared with the one corresponding to a thin constant mixing zone $\delta = 0.1$ (case $\delta(-50) = 0.1$). The results appear arranged in pairs corresponding to simulations at times $t = 30, 60, 120$ days. For both simulations, the interface is initially located on the diagonal. It then tends to a horizontal line due to density/gravity effects. Of course the results are similar on the right side of the aquifer. On the left side we observe that the mixing lessens the area of the aquifer occupied by saltwater.*

from the zone of diffusion back into the sea. The thickness of the latter zone is characterized by parameter δ in our model. We thus now consider higher values for δ. Furthermore, we test the possibility of varying δ in the domain since the mixing zone is thicker on the side of the shoreline. In Figure 7, the shoreline is on the left of the represented rectangle, a little further on. We impose homogeneous Neumann boundary conditions on the left of the domain in view of observing the free evolution of the interfaces depths due to water discharges. In accordance with [15], we observe that the salty interface get less elevated in the case of higher values for δ. If $\max \delta = \mathcal{O}(1)$ (which is not a drastic value) we observe a difference of 2% in the elevation. This effect is increasing over time.

Finally we couple the latter phenomenon with the tides effects. Tidal fluctuations of the sea produce progressive pressure waves in adjacent aquifers. Water-level measurements showing the landward decrease in tidal fluctuation are then often used for characterizing the physical parameters of groundwater flow (e.g., [28]). Of course this inverse process has to be based on adapted models. For this simulation we use the parameters in [15] after a rescaling to our small aquifer. We impose a Dirichlet boundary condition on the left boundary $\{x = -50\}$ for the saltwater elevation h. Its value is computed with the classical tide-produced change model for the artesian head of [19]. Parameter δ is calibrated using the formula for the amplitude of the dispersive zone ((2) in [15]). It is of order one. In the first figure we observe the tidal fluctuations in groundwater. Figure 8 presents actually two hydrograph artifacts showing the elevation of the salt interface over time. The oscillations appear of course if computations are performed on the model with $\delta = 0$ (on the left) or on the model with $\delta = \mathcal{O}(1)$ (on the right). In view of comparing the results between the
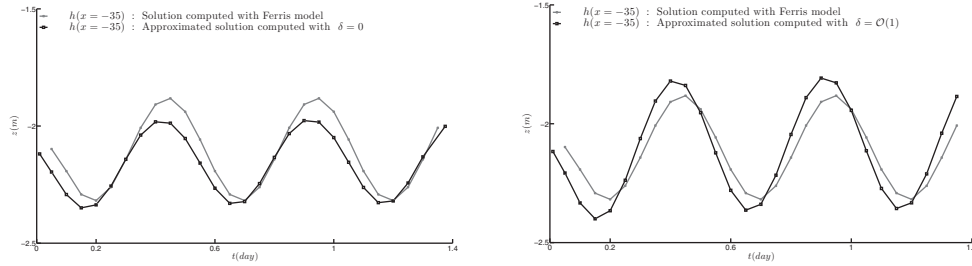
Fig. 8. *Tidal effects on the saltwater front depth h, represented by hydrograph artifacts (left $\delta = 0$, right $\delta = \mathcal{O}(1)$). The hydrograph is located at $x = -35$ m. An oscillating Dirichlet boundary condition, computed with the Ferris model, is imposed on the left of the domain for h (while H freely evolves with a homogeneous Neumann boundary condition on the left of the domain). Other parameters are those of [15]. The simulations are compared to the Ferris solution.*
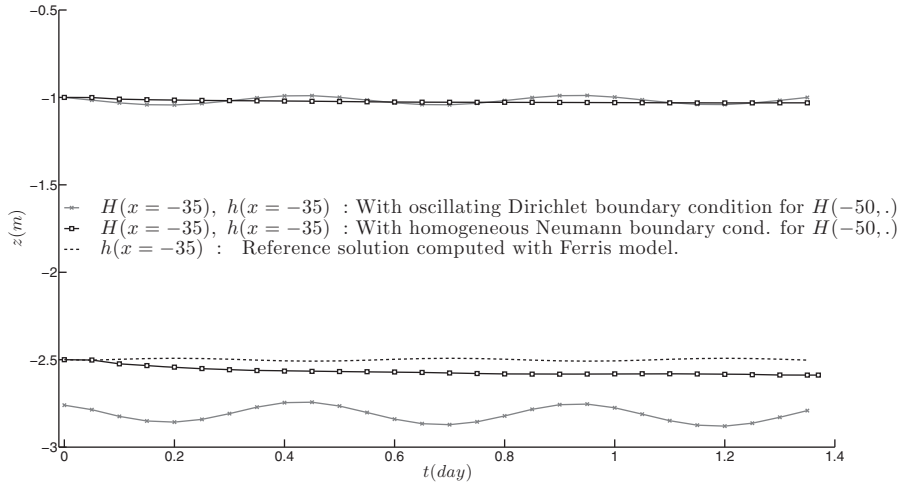

Fig. 9. *Impact of an oscillating Dirichlet boundary condition on H, simulations with $\delta = 0$. Artifact for a hydrograph at $x = -35$.*

two models, we thus have plotted a reference solution, here derived from the analytic formula of [19]. The curve produced by the model with $\delta \neq 0$ better fits the analytical solution. This observation is also confirmed at an other scale by the curves obtained with homogeneous Neumann boundary conditions in Figures 9 and 10.

The last figures are other phenomenological illustrations linked with tidal effects. First, in Figure 11, we focus on the water table elevation H. In the first subfigure we observe that the oscillations imposed on the left boundary of the aquifer on the saltwater front h induce an oscillating behavior on H. Moreover, as shown in the second subfigure, the sea tide has an enhancing effect on the mean water table of a coastal unconfined aquifer (see [20] and the references therein). In some ways Figures 9 and 10 present converse simulations since we illustrate the effects of the boundary condition chosen for H. Choosing an oscillating boundary condition or a Neumann boundary condition (knowing that oscillations are induced on H by the oscillating Dirichlet boundary condition on h) does not drastically impact the behavior of H. But it creates an important discrepancy on the saltwater front depth h. More precisely using the Dirichlet condition for H may produce the underestimate of h.
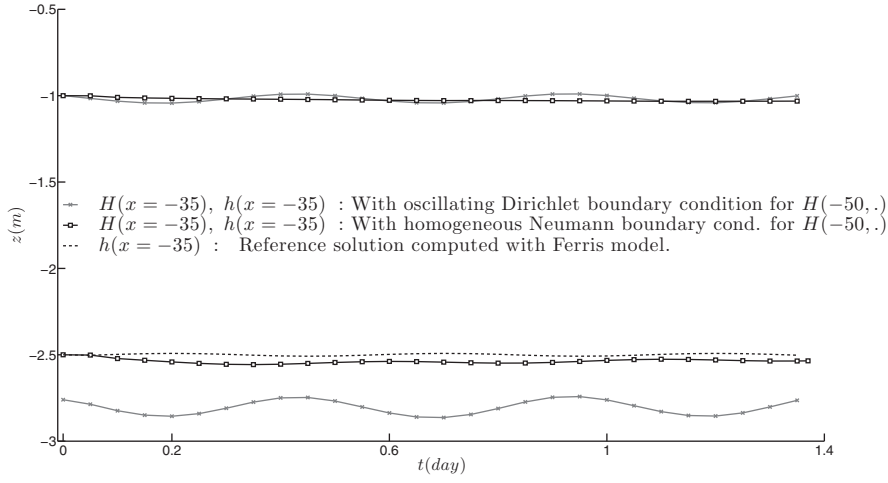
FIG. 10. *Impact of an oscillating Dirichlet boundary condition on H, simulations with $\delta = \mathcal{O}(1)$. Same data as in Figure 9.*
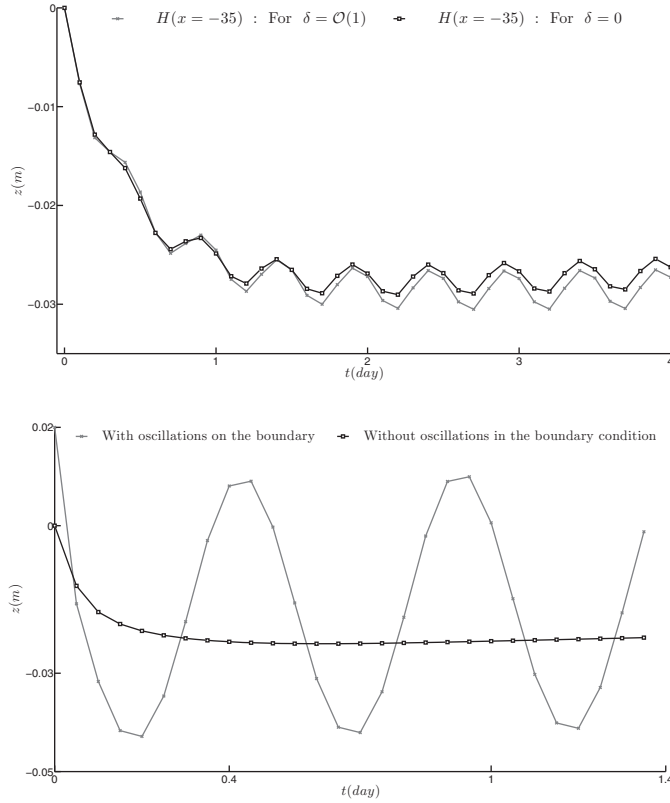

FIG. 11. *Tidal effects on the freshwater front depth H, represented by hydrograph artifacts. The data are the same as the ones used for Figure 8. The first subfigure shows the influence of δ on the oscillations. The second one illustrates the sea tide enhancing effect on the mean value of H.*

REFERENCES

[1] P. ACKERER AND A. YOUNES, *Efficient approximations for the the simulation of density driven flow in porous media*, Adv. Water Res., 31 (2008), pp. 15–27.

[2] M. ALFARO AND P. ALIFRANGIS, *Convergence of a mass conserving Allen-Cahn equation whose Lagrange multiplier is nonlocal and local*, Interfaces Free Bound., 16 (2014), pp. 243–268.

[3] M. ALFARO, D. HILHORST, AND M. HIROSHI, *Optimal interface width for the Allen-Cahn equation*, RIMS Kôkyûroku, 1416 (2005), pp. 148–160.

[4] Y. AMIRAT, K. HAMDACHE, AND A. ZIANI, *Mathematical analysis for compressible miscible displacement models in porous media*, Math. Models Methods Appl. Sci., 6 (1996), pp. 729–747.

[5] L.F. ATHY, *Density, porosity and compactation of sedimentary rocks*, Bull. Amer. Assoc. Petrol. Geol., 14 (1930), pp. 1–24.

[6] J. BEAR, A.H.D. CHENG, S. SOREK, D. OUAZAR, AND I. HERRERA, *Seawater Intrusion in Coastal Aquifers: Concepts, Methods and Practices*, Kluwer Academic, Dordrecht, 1999.

[7] J. BEAR AND A. VERRUIJT, *Modelling Groundwater Flow and Pollution*, D. Reidel, Dordecht, Holland, 1987.

[8] J. BEAR, *Dynamics of Fluids in Porous Media*, Elsevier, New York, 1972.

[9] G. BELLETTINI, L. BERTINI, M. MARIANI, AND M. NOVAGA, *Convergence of the one-dimensional Cahn–Hilliard equation*, SIAM J. Math. Anal., 44 (2012), pp. 3458–3480.

[10] A.J. BRAY, *Theory of phase-ordering kinetics*, Adv. Phys., 43 (1994), pp. 357–459.

[11] J.W. CAHN AND J.E. HILLIARD, *Free energy of non-uniform systems. I. Interfacial free energy*, J. Chem. Phys., 28 (1958), pp. 258–267.

[12] X. CHEN, *Global asymptotic limit of solution of the Cahn-Hilliard equation*, J. Differential Geom., 44 (1996), pp. 262–311.

[13] C. CHOQUET, *Parabolic and degerate parabolic models for pressure-driven transport problems*, Math. Models Methods Appl. Sci., 20 (2010), pp. 543–566.

[14] C. CHOQUET, M.M. DIÉDHIOU, AND C. ROSIER, *Mathematical analysis of a sharp-diffuse interfaces model for seawater intrusion*, J. Differential Equations, 259 (2015), pp. 3803–3824.

[15] H.H. COOPER, *A hypothesis concerning the dynamic balance of fresh water and salt water in a coastal aquifer*, U.S. Geological Survey Water-Supply Paper 1613-C, 1964, 1–12.

[16] M. DUBÉ, M. ROST, K.R. ELDER, M. ALAVA, S. MAJANIEMI, AND T. ALA-NISSILA, *Liquid conservation and nonlocal interface dynamics in imbibition*, Phys. Rev. Lett., 83 (1999), pp. 1628–1631.

[17] J. DUPUIT, *Études Théoriques et Pratiques sur le Mouvement des Eaux Dans les Canaux Couverts et à Travers les Terrains Perméables*, Dunod, Paris, 1863.

[18] H.L. ESSAID, *A multilayered sharp interface model of coupled freshwater and saltwater flow in coastal systems: Model developpement and application*, Water Res. Res., 26 (1990), pp. 1431–1454.

[19] J.G. FERRIS, *Cyclic fluctuations of water level as a basis for determining aquifer transmissibility*, Int. Assoc. Sci. Hydrol. Publ., 1 (1951), pp. 97–101.

[20] H. LI AND J.J. JIAO, *Analytical solutions of tidal groundwater flow in coastal two-aquifer systems*, Adv. Water Res., 25 (2002), pp. 417–426.

[21] P. MARION, K. NAJIB, AND C. ROSIER, *Numerical simulations for a seawater intrusion problem in a free aquifer*, Appl. Numer. Math., 75 (2014), pp. 48–60.

[22] A. NOVICK-COHEN, *The Cahn–Hilliard equation*, in Handbook of Differential Equations Vol. 4, C.M. Dafermos and E. Feireisl, eds., Elsevier, Amsterdam, 2008, pp. 201–228.

[23] O. PIRONNEAU, F. HECHT, AND A. LE HYARIC, *FreeFem++ version* 2.15-1, http://wwwfrefem.org/ff++/

[24] E.V. RADKEVICH, *On conditions for the existence of classical solution of the modified Stefan problem (The Gibbs–Thomson law)*, Sb. Math., 75 (1993), pp. 221–246.

[25] J. RUBINSTEIN AND P. STERNBERG, *Nonlocal reaction-diffusion equations and nucleations*, IMA J. Appl. Math., 48 (1992), pp. 249–264.

[26] J. RUBINSTEIN, P. STERNBERG, AND J.B. KELLER, *Fast reaction, slow diffusion, and curve shortening*, SIAM J. Appl. Math., 49 (1989), pp. 116–133.

[27] J. RUBINSTEIN, P. STERNBERG, AND J.B. KELLER, *Front interaction and non-homogeneous equilibria for tristable reaction-diffusion equations*, SIAM J. Appl. Math., 53 (1993), pp. 1669–1685.

[28] M. SERFES, *Determining the mean hydraulic gradient of ground water affected by tidal fluctuations*, Ground Water, 29 (1991), pp. 549–555.

[29] J. SHEN AND X. YANG, *A phase-field model and its numerical approximation for two-phase incompressible flows with different densities and viscosities*, SIAM J. Sci. Comput., 32 (2010), pp. 1159–1179.

[30] T. DOPPLER, H.J. HENDRICKS FRANSSEN, H.P. KAISER, U. KUHLMANN, AND F. STAUFFER, *Field evidence of a dynamic leakage coefficient for modelling river-aquifer interactions*, J. Hydrol., 347 (2007), pp. 177–187.

[31] M. SUSSMAN, K.M. SMITH, M.Y. HUSSAINI, M. OHTA, AND R. ZHI-WEI, *A sharp interface method for incompressible two-phase flows*, J. Comput. Phys., 221 (2007), pp. 469–505.

[32] M.H. TBER AND M.E. TALIBI, *A finite element method for hydraulic conductivity identification in a seawater intrusion problem*, Comput. Geosci., 33 (2007), pp. 860–874.

[33] K. TERZAGHI AND R.B. PECK, *Soil Mechanics in Engineering Practice*, Wiley, New York, 1967.